Neuron, Vol. 19, 1201–1210, December, 1997, Copyright ©1997 by Cell Press

NMDA Receptor-Dependent Refinement of Somatotopic Maps

Takuji Iwasato,* Reha S. Erzurumlu,† Patricio T. Huerta,* Dong Feng Chen,* Toshikuni Sasaoka,* Emel Ulupinar,† and Susumu Tonegawa*
*Howard Hughes Medical Institute
Center for Learning and Memory
Center for Cancer Research
Department of Biology
Massachusetts Institute of Technology
Cambridge, Massachusetts 02139
†Department of Cell Biology and Anatomy
LSU Medical Center
New Orleans, Louisiana 70112

Summary

We have examined the role of NMDA receptor–mediated neural activity in the formation of periphery-related somatosensory patterns, using genetically engineered mice. We demonstrate that ectopic expression of a transgene of an NMDAR1 splice variant rescues neonatally fatal *NMDAR1* knockout (KO) mice, although the average life span varies depending on the level of the transgene expression. In *NMDAR1* KO mice with "high" levels of the transgene expression, sensory periphery-related patterns were normal along both the trigeminal and dorsal column pathways. In the KO mice with "low" levels of the transgene expression, the patterns were absent in the trigeminal pathway. Our results indicate that NMDA receptor–mediated neural activity plays a critical role in pattern formation along the ascending somatosensory pathways.

Introduction

The somatosensory pathways of rodents have topographically ordered and patterned "somatotopic maps" in the primary somatosensory cortex (SI) and subcortical nuclei, which can be visualized by a number of histological stains. The trigeminal pathway and the dorsal column pathway are the major ascending projections in the rodent somatosensory system. The trigeminal pathway transmits somatosensory inputs from the face and oral structures to SI via the brainstem trigeminal complex (BSTC) and the ventral posterior medial (VPM) nucleus of the thalamus. The dorsal column pathway carries the somatosensory inputs from the rest of the body and involves the dorsal column nuclei of the brainstem and the ventral posterior lateral (VPL) nucleus of the thalamus (reviewed by Killackey et al., 1990). Along the trigeminal pathway, the afferent axons and target cells are organized in modules that replicate the patterned array of whiskers and sinus hairs on the animal's snout (Woolsey and Van der Loos, 1970; Van der Loos, 1976; Belford and Killackey, 1979; Ma and Woolsey, 1984). These modules are called "barrels" in SI, "barreloids" in VPM, and "barrelettes" in BSTC. A similar patterned organization is observed in the forepaw representation areas along the dorsal column pathway leading to SI (Belford and Killackey, 1978; Dawson and Killackey, 1987).

The cellular and molecular mechanisms underlying the formation of sensory periphery-related patterns are not well understood. Increasing evidence indicates that molecular interactions between axons and targets set the stage for topographic connections, and neural activity mediates further refinement or patterning of sensory maps (Goodman and Shatz, 1993; Katz and Shatz, 1996). In particular, it is thought that N-methyl-D-aspartate (NMDA) receptors are critically involved in the latter process (Goodman and Shatz, 1993; Cramer and Sur, 1995; Katz and Shatz, 1996). However, most of the evidence in support of the role of neural activity in the refinement or patterning of sensory periphery-related maps comes from pharmacological studies in the visual system (Stryker and Harris, 1986; Shatz and Stryker, 1988; Hahm et al., 1991). For the somatosensory system, earlier studies indicated that pharmacological blockade of neural activity or NMDA receptor function in the neocortex or infraorbital nerve does not disrupt pattern formation in the rat trigeminal system (Chiaia et al., 1992; Henderson et al., 1992; Schlaggar et al., 1993). Recently, Fox et al. (1996) showed that local application of an NMDA receptor antagonist (AP5) to the neocortex at postnatal day 0 (P0) does not noticeably modify the barrel pattern but disrupts the one-to-one functional relationship between whiskers and barrels. On the other hand, Mitrovic et al. (1996) reported that application of NMDA receptor antagonists (AP5 and MK801) systemically by intraperitoneal injection or locally to the neocortex at P2 produces abnormalities in the morphological appearance of barrels and the segregation of thalamocortical afferents. Thus, a consensus is yet to be reached on the role of neural activity in patterning of somatotopic maps.

We have been reinvestigating this issue by constructing and analyzing NMDA receptor knockout (KO) mice. Each NMDA receptor is composed of the NMDAR1 (NR1) subunit and at least one of four NR2 (A to D) subunits (Nakanishi, 1992). Li et al. (1994) produced knockout mice of the NR1 subunit, rendering NMDA receptors functionally ineffective. The *NR1* KO mice die within a day after birth (Forrest et al., 1994; Li et al., 1994). However, the life span of these mice could be prolonged up to P2 by artificially delayed birth and respiratory stimulation. It was shown that barrelettes were absent in the *NR1* KO mice at P2, even though other aspects of somatotopic map formation such as pathfinding and topographic organization of trigeminal afferents were normal in BSTC (Li et al., 1994). This study provided the first direct evidence for the involvement of NMDA receptors in periphery-related patterning of neural elements within somatotopic maps in the trigeminal brainstem. Similar results were subsequently obtained with *NR2B* KO mice (Kutsuwada et al., 1996, T. S. et al., unpublished data).

While these studies clearly demonstrated the effects of the knockout of an NMDA receptor gene in the BSTC, the possibility that the pattern formation was delayed

rather than abolished could not be excluded because of the short life span of the *NR1* KO mice (O'Leary et al., 1994). For the same reason, pattern formation at higher somatosensory centers (e.g., VPM and SI) could not be examined. To address these issues, we attempted to rescue the *NR1* KO mice by ectopic expression of an *NR1* transgene. Our assumption was that we may be able to produce mice in which the level of the expression of the transgenic *NR1* gene is high enough to prolong life but is insufficient for pattern formation. We found this to be the case. Our results indicate that NMDA receptor-mediated processes are critically involved in pattern formation in the somatosensory system.

Results

Introduction of an *NR1* Transgene with "High" Levels of Expression into *NR1* KO Mice ($NR1^{-/-}HTg^{+/-}$ Mice)

Relatively high levels of NR1 expression were accomplished by employing a transgene in which a modified chicken β-actin promoter (*CAG* promoter; Niwa et al., 1991) drove the expression of the *NR1-1a* (an NR1 splice variant; Zukin and Bennett, 1995) cDNA sequence (Figure 1A, construct *pCAG-NR1*). Eighteen out of the 21 founder mice transmitted the transgene through the germline. We compared the levels of transgenic *NR1* mRNA in 13 lines by Northern blot analysis using a transgene-specific probe (probe-T, Figure 1A) and chose three lines (C26, C27, and C28) that displayed the highest levels of expression in the adult brain (data not shown). We mainly used the transgene-heterozygous C28 line ($C28^{+/-}$ or $HTg^{+/-}$) for further studies. Northern blot analysis showed that expression of the transgene is widely distributed in the developing brain of the $HTg^{+/-}$ mice (Figure 1B). By mating the $HTg^{+/-}$ mice with heterozygous *NR1* KO mice ($NR1^{+/-}$ mice), we obtained $NR1^{+/-}HTg^{+/-}$ mice, which were then backcrossed to the $NR1^{+/-}$ mice. In adult mice generated by the latter type of crosses, we found transgenic mice in the homozygous *NR1* KO background ($NR1^{-/-}HTg^{+/-}$ mice), indicating that the expression of an *NR1-1a* transgene could rescue the *NR1* KO mice. We also obtained adult mice from the *NR1* transgenic lines C26 and C27 in the $NR1^{-/-}$ background.

At 3 weeks of age, $NR1^{-/-}HTg^{+/-}$ mice appeared normal except for their relatively small size, but as they got older, many became wasting and spastic. $NR1^{-/-}HTg^{+/-}$ males and females were fertile but were poor breeders. We analyzed genotypes of 64 newborn pups derived by in vitro fertilization between $NR1^{-/-}HTg^{+/-}$ mice and $NR1^{+/-}$ mice and found 20 $NR1^{-/-}HTg^{+/-}$, 15 $NR1^{+/-}HTg^{+/-}$, 15 $NR1^{-/-}HTg^{-/-}$, and 14 $NR1^{+/-}HTg^{-/-}$ mice. These results indicate that embryos generated by this type of crosses could develop to term with no obvious bias against any of the expected genotypes. We closely observed the development of the 17 $NR1^{-/-}HTg^{+/-}$ newborn pups and found that all except three grew to adulthood (older than 3 months). One mouse died at P0 and two at P1. The average body weight of the $NR1^{-/-}HTg^{+/-}$ mice was slightly lower than that of littermates of the other genotypes: $NR1^{-/-}HTg^{+/-}$, $NR1^{+/-}HTg^{+/-}$, and $NR1^{+/-}HTg^{-/-}$ mice weighed on average 16.88 ± 1.93 g (n = 12), 21.45 ± 3.23 g (n = 6), and 22.81 ± 2.53 g (n = 12), respectively (at P35).

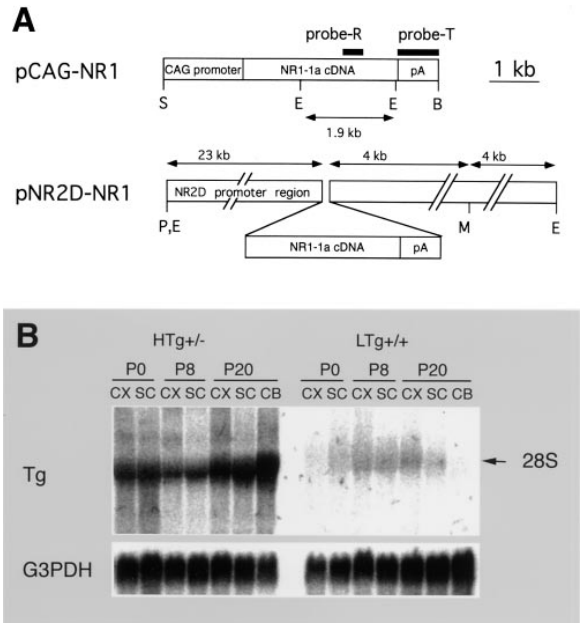

Figure 1. Production of *NR1* Transgenic Mice

(A) The transgenic constructs. *pCAG-NR1* carries a strong constitutive promoter (*CAG* promoter), rat *NR1-1a* cDNA, and SV40 early splice region/polyadenylation signal (pA). *pNR2D-NR1* carries a putative *NR2D* promoter region and NR1-1a/pA. Transgenic lines HTg and LTg were generated by injecting the SalI-BamHI fragment of *pCAG-NR1* and the PacI-MluI fragment of *pNR2D-NR1* constructs, respectively, into fertilized eggs. Probe-R is designed to detect transgenic NR1 and wild-type NR1 but not mutant NR1. Probe-T is specific to the transgenes. Abbreviations for restriction enzyme sites: S, SalI; E, EcoRI; B, BamHI; P, PacI; M, MluI. Some EcoRI sites on the *CAG* promoter and *NR1-1a* cDNA and SalI and BamHI sites on the *NR2D* promoter region are not shown.

(B) Northern blot analysis of transgene expression in developing transgenic mice. Twenty micrograms of total RNA was loaded per lane, blotted, and hybridized with probe-T (top). The same blot was rehybridized with glycerol-3-phosphate dehydrogenase (G3PDH) probe as a control for the amount of RNA loaded (bottom). Bands in lanes of $LTg^{+/+}$ mice are broad, probably because of multiple transcriptional initiation sites and/or alternative splicing. Expression levels of transgenes in $LTg^{+/+}$ mice were much lower than those in $HTg^{+/-}$ mice throughout development. Abbreviations: CX, cortical region (cerebral cortex, hippocampus, striatum); SC, subcortical region (diencephalon and brainstem); CB, cerebellum.

In situ hybridization of P0 (data not shown) and P8 brain slices (Figure 2A) with an NR1-specific probe (probe-R, Figure 1A) showed that the *NR1* gene was expressed widely in $NR1^{-/-}HTg^{+/-}$ brains. Levels of expression of the *NR1* gene in $NR1^{-/-}HTg^{+/-}$ mice were slightly lower than or similar to those in wild-type mice (Figures 2A and 2B, right).

Introduction of an *NR1* Transgene with "Low" Levels of Expression into *NR1* KO Mice ($NR1^{-/-}LTg^{+/+}$ Mice)

We also produced *NR1* transgenic mice by driving the expression of the *NR1-1a* cDNA sequence with a second promoter, 27 kb sequence from the upstream region

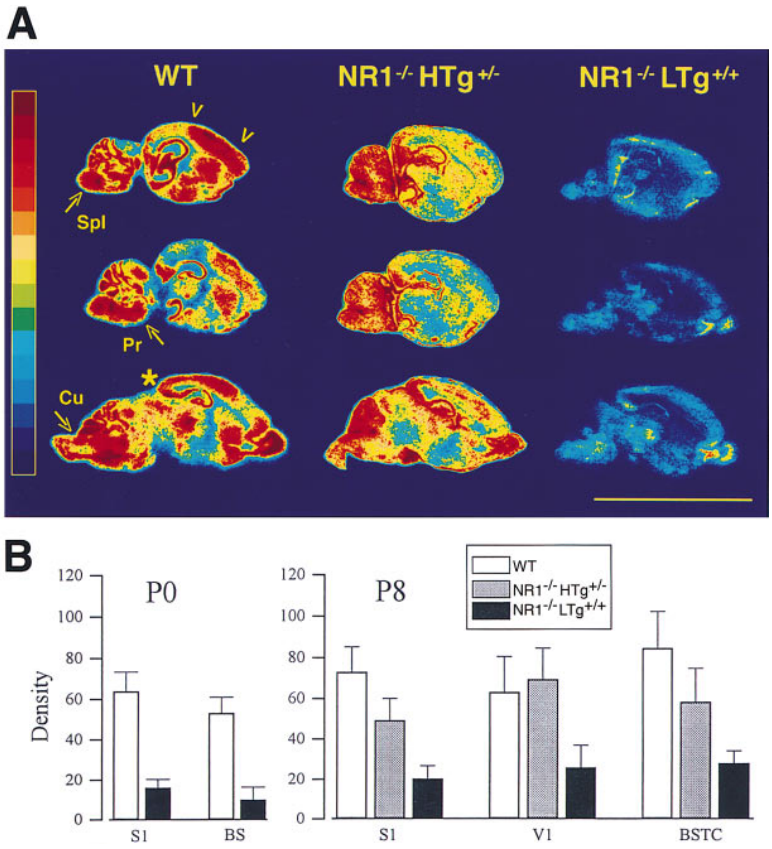

Figure 2. In Situ Hybridization Studies of Rescued Mice

(A) Probe-R (Figure 1A) was used. Sagittal views of wild-type (WT), *NR1*$^{-/-}$*HTg*$^{+/-}$, and *NR1*$^{-/-}$*LTg*$^{+/+}$ mice at P8. The sections were processed simultaneously and exposed to a single X-ray film. Brain sections of an *NR1* knockout mouse (negative control), which were processed together, did not have any detectable signals (no background; data not shown). Arrows show the subnucleus interpolaris (SpI) and principal nucleus (Pr) of brainstem trigeminal complex (BSTC) and cuneate nucleus (Cu). Arrow heads show SI. An asterisk shows the primary visual cortex (VI). Scale bar, 1 cm.

(B) Densitometric measurement of levels of NR1 expression in brain subregions. Expression levels of wild-type mice might be slightly underestimated, because the probe (probe-R) was derived from a rat *NR1* cDNA (94% nucleotide homology with mouse in the corresponding region). BS, brainstem.

of the *NR2D* gene (Figure 1A, PacI-MluI fragment of construct *pNR2D-NR1*). We chose the transgene-homozygous N14 line (*N14*$^{+/+}$ or *LTg*$^{+/+}$ line) out of 13 germline-transmitting lines for further studies. Northern blot analysis showed that the expression of the *NR1* transgene in the *LTg*$^{+/+}$ line was lower than in the *HTg*$^{+/-}$ line and also more restricted in terms of tissue distribution (Figure 1B). Thus, while the expression was detectable in both cortical and subcortical regions at P0, P8, and P20 in *LTg*$^{+/+}$ mice, the levels were between 7.5% and 46% of those of the corresponding regions in the *HTg*$^{+/-}$ mice of the corresponding ages. In addition, *NR1* mRNA was barely detectable in the cerebellum of P20 *LTg*$^{+/+}$ mice, while it was abundant in the cerebellum of P20 *HTg*$^{+/-}$ mice.

We crossed the *LTg*$^{+/-}$ mice with heterozygous *NR1* KO mice (*NR1*$^{+/-}$ mice) and obtained *NR1*$^{+/-}$*LTg*$^{+/-}$ mice, which were then backcrossed to the *LTg*$^{+/-}$ mice to get *NR1*$^{+/-}$*LTg*$^{+/+}$ mice. The intercrosses of the latter mice resulted in a total of 177 P0 pups (born among 25 litters), whose genotypes were 49 *NR1*$^{+/+}$*LTg*$^{+/+}$, 84 *NR1*$^{+/-}$*LTg*$^{+/+}$, and 44 *NR1*$^{-/-}$*LTg*$^{+/+}$. The ratio of these numbers is close to 1:2:1, suggesting that there is no selection against the development of the embryos in any of the three genotypes. However, 22 of 31 *NR1*$^{-/-}$*LTg*$^{+/+}$ pups died at P0. Although the body weight of the *NR1*$^{-/-}$*LTg*$^{+/+}$ mice was not significantly different from that of littermates at P0, their growth rate was relatively low. At P8, the average body weight was 3.81 ± 1.15 g (n = 9), 6.23 ± 0.84 g (n = 16), and 5.79 ± 0.87 g (n = 17) for *NR1*$^{-/-}$*LTg*$^{+/+}$, *NR1*$^{+/-}$*LTg*$^{+/+}$, and *NR1*$^{+/+}$*LTg*$^{+/+}$ mice, respectively. The *NR1*$^{-/-}$*LTg*$^{+/+}$ mice were active. Typically after 2 weeks of age, they began to lose their body weight and eventually died in a severely emaciated state, although the primary cause of this physical degeneration is not known. Out of nine rescued mice, one died at P9, seven died between P18 and P24, and the other died at P63. Overall brain structure of *NR1*$^{-/-}$*LTg*$^{+/+}$ mice appeared normal at P8 and P17 (data not shown). In SI, the relative thickness of layers I–VI also appeared normal.

In situ hybridization analysis of brain sections derived from P0 (data not shown) and P8 (Figure 2A) *NR1*$^{-/-}$*LTg*$^{+/+}$ mice showed that *NR1* mRNA was detectable at low levels in the cortex, diencephalon, and brainstem but was absent in the cerebellum and some other parts of the brain. We compared the expression levels of *NR1* mRNA in the cortical and subcortical regions using a computer image analysis system (N.I.H. Image 1.6). The levels of NR1 expression in SI and the brainstem (BS) of *NR1*$^{-/-}$*LTg*$^{+/+}$ mice at P0 were lower than those in the corresponding regions of wild-type mice (Figure 2B, left). The levels of NR1 expression in SI, the primary visual cortex (VI), and BSTC of *NR1*$^{-/-}$*LTg*$^{+/+}$ mice at P8 were also lower than those in the corresponding regions of wild-type mice and *NR1*$^{-/-}$*HTg*$^{+/-}$ mice (Figure 2B, right). High power images from emulsion-dipped slides showed that the levels of NR1 expression in layer IV of SI, the principal nucleus (Pr) and subnucleus interpolaris (SpI) of BSTC, and the cuneate nucleus (Cu) of the dorsal column nuclei of *NR1*$^{-/-}$*LTg*$^{+/+}$ mice were much lower than those in the corresponding regions of

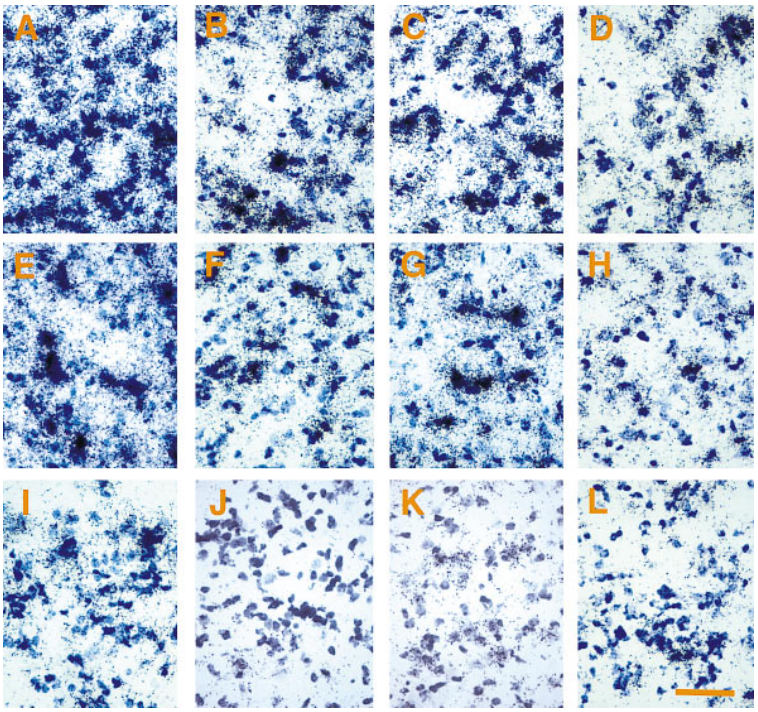

Figure 3. Bright-Field Photographs of Emulsion-Dipped Sections

NR1 expression in layer IV of SI (A, E, and I), Pr (B, F, and J), SpI (C, G, and K), and Cu (D, H, and L) of wild-type (A–D), *NR1*$^{-/-}$*HTg*$^{+/-}$ (E–H), and *NR1*$^{-/-}$*LTg*$^{+/+}$ (I–L) mice at P8. The levels of NR1 expression in SI, Pr, SpI, and Cu of *NR1*$^{-/-}$*LTg*$^{+/+}$ mice were much lower than those in the corresponding regions of wild-type and *NR1*$^{-/-}$*HTg*$^{+/-}$ mice. In *NR1*$^{-/-}$*LTg*$^{+/+}$ mice, Pr showed extremely low levels of NR1 expression (J), while SpI (lateral part) (K) and Cu (L) showed relatively high levels of expression. Scale bar, 50 μm.

wild-type and *NR1*$^{-/-}$*HTg*$^{+/-}$ mice (Figure 3). Interestingly, within the brainstem of *NR1*$^{-/-}$*LTg*$^{+/+}$ mice, we found differential levels of expression of the *NR1* mRNA. Pr had very low levels of *NR1* mRNA expression (Figure 3J). Within SpI, only the lateral part had relatively high levels of *NR1* mRNA expression (Figure 3K), whereas other regions of the nucleus showed very low levels (data not shown), similar to those seen in Pr. Finally, the *NR1* mRNA expression in Cu was relatively high (Figure 3L).

Reduced NMDA Receptor–Dependent Responses in Layer IV Neurons of SI in *NR1*$^{-/-}$*LTg*$^{+/+}$ Mice

To investigate whether the transgenic *NR1* gene restores NMDA receptor function in the *NR1* KO mice, we examined the presence of NMDA-mediated synaptic responses in layer IV neurons of SI that receive direct input from the thalamus. We used the thalamocortical slice preparation (Figure 4A) developed by Agmon and Connors (1991) to record from identified layer IV neurons under visual guidance (reviewed in Sakmann and Stuart, 1995). We measured excitatory postsynaptic currents (EPSCs) during whole-cell patch-clamp recordings upon stimulation of the thalamic afferents. Slices from wild-type (n = 10, four mice), *NR1*$^{-/-}$*HTg*$^{+/-}$ (n = 11, four mice), and *NR1*$^{-/-}$*LTg*$^{+/+}$ mice (n = 15, five mice) were examined.

The synaptic responses in neurons from the *NR1*$^{-/-}$*HTg*$^{+/-}$ mice were similar to those of wild-type mice (Figure 4B). The isolated fast component of the EPSC, which corresponds to the AMPA-mediated response, was abolished by the antagonist DNQX (10 μM) and showed a current-to-voltage (I-V) relation comparable to wild-type neurons (data not shown). The slow component, which represents the NMDA receptor–mediated response, was blocked by AP5 and showed an I-V relation similar to wild-type neurons (Figure 4B, right).

The synaptic responses measured in *NR1*$^{-/-}$*LTg*$^{+/+}$ neurons showed that the fast, AMPA-mediated component was similar to that of wild-type mice (data not shown). In contrast, the slow NMDA-dependent responses were expressed in a diminished way in the *NR1*$^{-/-}$*LTg*$^{+/+}$ neurons (Figure 4B). The I-V relation for the isolated NMDA EPSCs showed that these currents were significantly smaller in *NR1*$^{-/-}$*LTg*$^{+/+}$ neurons compared to wild-type or *NR1*$^{-/-}$*HTg*$^{+/-}$ neurons (Figure 4B, right). The synaptic responses in *NR1*$^{-/-}$*LTg*$^{+/+}$ neurons were indeed NMDA-dependent because they were completely blocked by the antagonist AP5 (50 μM) (Figure 4C). Finally, we computed the ratio of NMDA responses to AMPA responses in each type of mouse and found that the ratio for the *NR1*$^{-/-}$*LTg*$^{+/+}$ mutants was 27% of that of wild-type mice (Figure 4D).

Absence of Whisker-Related Patterns in SI and Subcortical Nuclei of *NR1*$^{-/-}$*LTg*$^{+/+}$ Mice

To examine the periphery-related pattern formation along the somatosensory pathways of *NR1*$^{-/-}$*LTg*$^{+/+}$ mice, cytochrome oxidase (CO) histochemistry was carried out (Figure 5). Some experiments were done in a blind fashion. In *NR1*$^{-/-}$*LTg*$^{+/+}$ mice (n = 12 at P8), the dense overall CO staining delineated the body and face representation areas in SI, indicating that the overall orientation and shape of the somatotopic maps are not altered. But importantly, the whisker-related pattern was absent (Figure 5C). Interestingly, the adjacent forepaw-related region displayed a normal pattern corresponding to digits and palm pads. In the thalamus, there were no detectable barreloids in VPM, but there was normal forepaw-related segmentation in VPL (Figure 5F). In

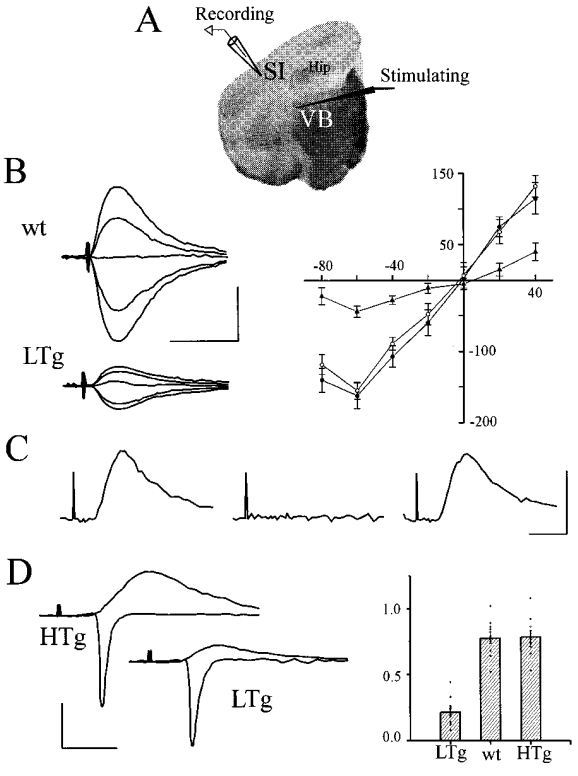

Figure 4. NMDA Receptor-Dependent Responses in SI

(A) Diagram of the thalamocortical slice. The stimulating electrode was placed in the ventrobasal (VB) nucleus of the thalamus and the recording electrode in layer IV of SI. Whole-cell recordings were made from neurons in layer IV that receive monosynaptic input form the thalamus (see Experimental Procedures). Hip, hippocampus.

(B) Isolated NMDAR-dependent synaptic responses upon thalamic stimulation. The left panel shows EPSCs recorded at different holding voltages (-60, −40, 0, 20, 40 mV) from wild-type (wt) and *NR1*$^{-/-}$*LTg*$^{+/+}$ (LTg) mice; each trace is an average of 20 individual sweeps. NMDA currents were isolated by addition of CNQX (20 μM), picrotoxin (100 μM), 2-OH-saclofen (200 μM), and by removing Mg^{2+} from the saline solution. Scale, 100 ms, 100 pA. The right panel shows current-to-voltage plots for NMDAR EPSCs from wild-type (n = 15 cells, open circles), *NR1*$^{-/-}$*HTg*$^{+/-}$ (n = 10 cells, closed circles), and *NR1*$^{-/-}$*LTg*$^{+/+}$ (n = 15 cells, closed triangles) mice. Symbols represent mean ± SEM.

(C) NMDAR EPSCs from *NR1*$^{-/-}$*LTg*$^{+/+}$ mice are blocked by AP5. Representative responses before (left), during bath application of 50 μM AP5 (middle), and after washout (right). Scale, 100 ms, 25 pA.

(D) Ratio of NMDA over AMPA-dependent EPSCs in the *NR1*$^{-/-}$*HTg*$^{+/-}$ (HTg) and *NR1*$^{-/-}$*LTg*$^{+/+}$ (LTg) mice. The left panel shows representative examples of isolated AMPA EPSCs (downward curve; holding potential, −90 mV) and NMDA EPSCs (upward curve; holding potential, 40 mV). Scale, 25 ms, 100 pA. The mean values were: AMPA currents (pA) 201 ± 38 (n = 10), 194 ± 27 (n = 11), 187 ± 25 (n = 13) and NMDA currents (pA) 156 ± 13, 152 ± 18, 40 ± 6, for wild-type, *NR1*$^{-/-}$*HTg*$^{+/-}$, and *NR1*$^{-/-}$*LTg*$^{+/+}$, respectively. The right panel shows the ratio of NMDA/AMPA responses for the three different lines of mice. The bars represent average values and the dots, individual measurements.

BSTC, Pr (Figure 5I) and SpC (subnucleus caudalis) (data not shown) did not exhibit any barrelettes, although these areas were densely stained. SpI showed five rows of rudimentary barrelettes only in the lateral portion of the nucleus (Figure 5L). In the dorsal column nuclei, Cu had normal forepaw-related segmentation (data not shown). These phenotypes were consistent, and we did not see a single case that varied from the others. Disruption of the whisker-related cortical pattern was confirmed by Nissl and NADPH-diaphorase (NADPH-d) stains (Figures 6A–6D). Nissl and NADPH-d stains showed the absence of cell clusters and the absence of NADPH dense patches, respectively, in the layer IV of SI.

We compared pattern formation of large *NR1*$^{-/-}$*LTg*$^{+/+}$ (4.89 ± 0.24 g, n = 5), small *NR1*$^{-/-}$*LTg*$^{+/+}$ (2.84 ± 0.73 g, n = 7), normal size control (5.28 ± 1.01 g, n = 12), and small control pups (2.37 ± 0.38 g, n = 8), all at P8, by using CO staining. We did not find any difference in pattern formation in mice with the same genetic background despite differences in body weight. We also examined the whisker-related patterns in 2- to 4-week-old *NR1*$^{-/-}$*LTg*$^{+/+}$ mice (n = 6), and the results were similar to that seen at P8 (data not shown). Hence, the disrupted pattern along the trigeminal pathway of *NR1*$^{-/-}$*LTg*$^{+/+}$ mice is not due to developmental retardation. It is also unlikely that ectopic expression of the *NR1* gene in *NR1*$^{-/-}$*LTg*$^{+/+}$ was responsible for the pattern disruption. We have examined *LTg*$^{+/+}$ mice with wild-type or heterozygous *NR1* KO backgrounds (*NR1*$^{+/+}$*LTg*$^{+/+}$ or *NR1*$^{+/-}$*LTg*$^{+/+}$) at P8 (n = 8) and P43 (n = 1) by CO staining and found that all of them had normal patterns at every level of the somatosensory pathway (data not shown).

In a second series of anatomical experiments, the lipophilic tracer DiI was used to examine the afferents along the trigeminal pathway in normal (n = 8) and *NR1*$^{-/-}$*LTg*$^{+/+}$ mice (n = 8) at P5 (Figures 6E–6H). DiI crystals were applied to either the trigeminal ganglion, Pr, or VPM, and axonal labeling in the brainstem trigeminal nuclei, VPM, or barrel cortex, respectively, was examined. In the flattened cortex of *NR1*$^{-/-}$*LTg*$^{+/+}$ mice, thalamic projections appeared normal in their density and distribution within the target, but afferent terminals were not clustered into periphery-related patterns (Figure 6F) as they are in normal mice. In the coronally sectioned cortex of *NR1*$^{-/-}$*LTg*$^{+/+}$ mice, these afferents formed a dense and continuous band in layer IV without any hints of segmentation (Figure 6H). Apparently normal axonal projections, but without whisker-specific patterning, were also observed in VPM and BSTC (data not shown).

Introduction of an *NR1* Transgene with "Very Low" Levels of Expression into *NR1* KO Mice (*NR1*$^{-/-}$*LTg*$^{+/-}$ Mice)

NR1$^{-/-}$ mice with the N14 transgenic *NR1* gene on an allele (*NR1*$^{-/-}$*LTg*$^{+/-}$ mice) express *NR1* mRNA at levels even lower than *NR1*$^{-/-}$*LTg*$^{+/+}$ mice. Northern blot analysis using a transgene-specific probe (probe-T, Figure 1A) showed that levels of transgene expression in *LTg*$^{+/-}$ mice were about half of those of the *LTg*$^{+/+}$ mice (data not shown). We mated *NR1*$^{+/-}$*LTg*$^{+/+}$ mice with *NR1*$^{+/-}$*LTg*$^{-/-}$ mice on a large scale. Out of 217 P0 pups (from 31 litters), we found 58 *NR1*$^{-/-}$*LTg*$^{+/-}$. Among them, only one survived for more than 1 day, even though for these matings we used many mothers that were able to nurse *NR1*$^{-/-}$*LTg*$^{+/+}$ pups. In the subsequent 57 litters, we did

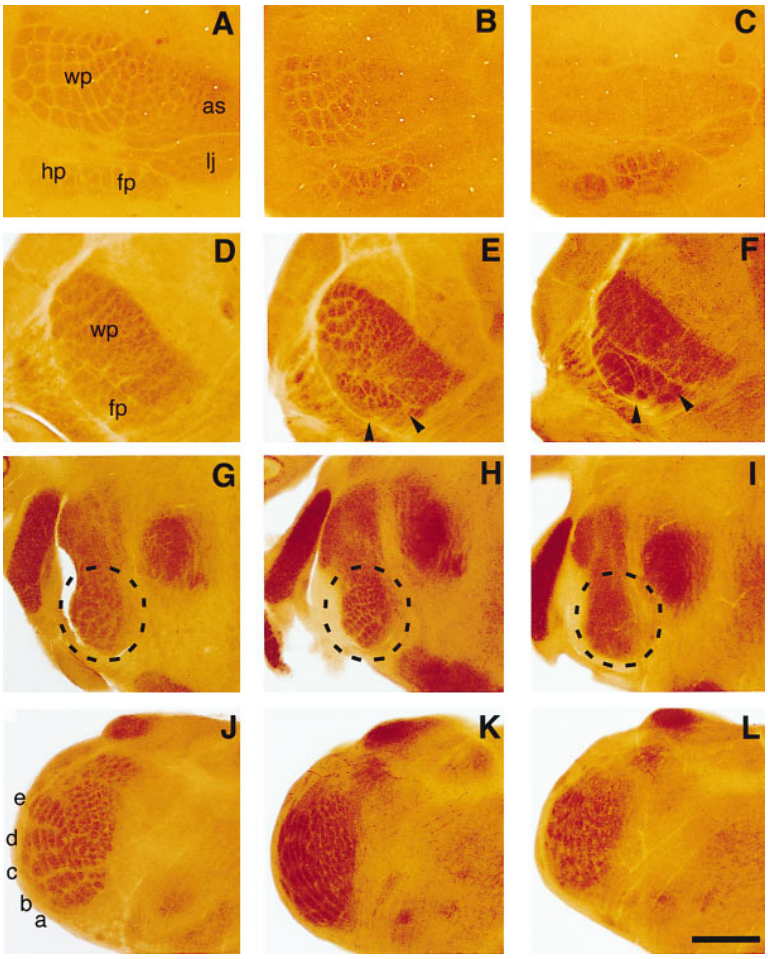

Figure 5. CO Staining of P8 Brains

(A–C) Flattened sections of cortex. In both the wild-type (A) and *NR1*$^{-/-}$*HTg*$^{+/-}$ (B) mice, five rows of whisker-related pattern and forepaw-related segmentation are similar. In *NR1*$^{-/-}$*LTg*$^{+/+}$ mice (C), whisker pattern is absent, but the forepaw segmentation is present. Note that the face and lower jaw representation areas can be visualized (C).

(D–F) Coronally sectioned thalamus. Whisker pattern (wp) and forepaw segmentation (fp) (indicated by arrow heads) are apparent in the wild-type (D) and *NR1*$^{-/-}$*HTg*$^{+/-}$ (E) mice. In *NR1*$^{-/-}$*LTg*$^{+/+}$ mice, barreloids are absent, but the forepaw segmentation is present (F).

(G–I) Coronally sectioned principal nucleus (Pr). In the ventral Pr (indicated by circles), five rows of barrelettes are seen in the wild-type (G) and *NR1*$^{-/-}$*HTg*$^{+/-}$ (H) mice, but this pattern is absent in the *NR1*$^{-/-}$*LTg*$^{+/+}$ mice (I). However, the entire Pr is stained densely (I).

(J–L) Coronally sectioned subnucleus interpolaris (SpI). Barrelettes are similar in both the wild-type (J) and *NR1*$^{-/-}$*HTg*$^{+/-}$ (K) mice. A rudimentary barrelette pattern could be detected in the *NR1*$^{-/-}$*LTg*$^{+/+}$ mice (L). Barrelette rows (a–e) are indicated in (J); wp, whiskerpad representation; as, anterior snout; lj, lower jaw; hp, hindpaw; fp, forepaw.

Scale bar, 800 μm for (A)–(C) and 400 μm for (D)–(L).

not find any *NR1*$^{-/-}$*LTg*$^{+/-}$ mice that survived beyond P1. Thus, the survival frequency (longer than 1 day) of *NR1*$^{-/-}$*LTg*$^{+/-}$ mice was distinctly lower than that of *NR1*$^{-/-}$*LTg*$^{+/+}$ mice. The surviving *NR1*$^{-/-}$*LTg*$^{+/-}$ pup was healthy but small in size (3.38 g at P8), similar to the *NR1*$^{-/-}$*LTg*$^{+/+}$ mice.

We examined the trigeminal and dorsal column pathways of this mouse at P8 by NADPH-d and CO staining (Figure 7) and found no whisker-related patterns in SI (Figures 7B and 7C), VPM (Figure 7D), Pr, and SpC (data not shown). In SpI, an immature patterning without any indication of rows was barely detectable (data not shown). Moreover, no detectable patterns could be observed along the dorsal column pathway (Figures 7B–7D and 7F). Because all *NR1*$^{-/-}$*LTg*$^{+/+}$ mice (P8, n = 12) had normal forepaw patterns at all levels and five rows of immature barrelettes in SpI, we think these differences are significant, even though the study was limited to only one *NR1*$^{-/-}$*LTg*$^{+/-}$ mouse.

Restored Somatotopic Patterns in *NR1*$^{-/-}$*HTg*$^{+/-}$ Mice

We examined whether high levels of expression of a transgene of an NR1 splice variant, *NR1-1a*, not only rescues *NR1* KO mice but also mediates the pattern formation in the somatosensory system. We found that both the whisker-related barrels and the forepaw-related segmentation were normal in SI of the *NR1*$^{-/-}$*HTg*$^{+/-}$ mice at P8 (n = 9, Figure 5B) and older ages (P17 to adult: n = 8, data not shown). In the thalamus, we observed the whisker-related barreloids in VPM and forepaw-related segmentation in VPL (Figure 5E). In the brainstem, Pr (Figure 5H), SpI (Figure 5K), and SpC (data not shown) as well as Cu (data not shown) showed normal patterns. These observations were not peculiar to the single NR1 transgenic line C28, because at least two other lines, C26 and C27, also promoted the formation of somatotopic patterns in SI in the *NR1*$^{-/-}$ background (data not shown).

Discussion

We previously produced *NR1* KO mice in order to test the hypothesis that NMDA receptor–mediated activity is required for pattern formation in the somatosensory system (Li et al., 1994). However, these mice could not be kept alive beyond P2, so analysis was limited to BSTC, in which the patterns are formed relatively early in development compared to the thalamus or SI. In *NR1* KO mice, focal applications of the lipophilic axonal tracer DiI to different rows of developing whisker follicles in early and late embryonic mice revealed that topographic projections of trigeminal axons between the whisker pad and the brainstem trigeminal nuclei were

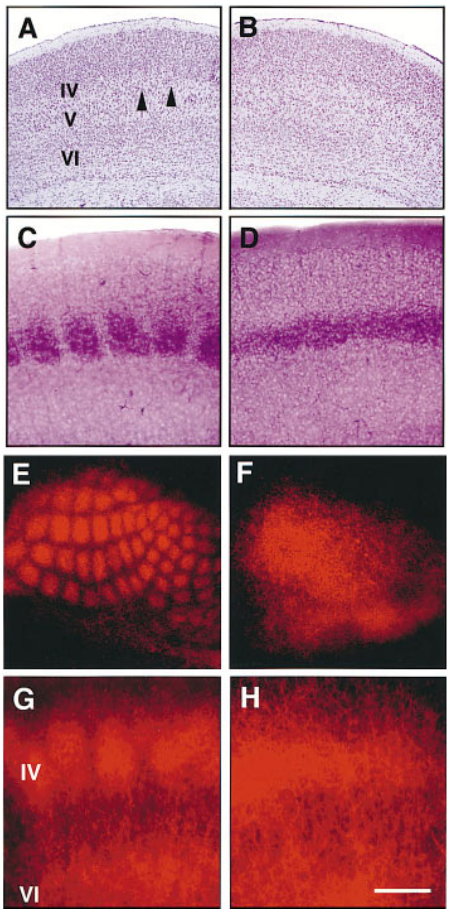

Figure 6. Cortical Barrels And Distribution of Thalamocortical Afferents in Wild-Type and *NR1*$^{-/-}$*LTg*$^{+/+}$ Mice

(A and B) Cytoarchitectonic differences observed in the coronal plane with Nissl stain. In wild-type mice, aggregates of granule cells in layer IV form whisker-specific barrels (A, arrow heads). These cellular aggregates are absent in layer IV of the *NR1*$^{-/-}$*LTg*$^{+/+}$ mice (B). Note that the relative thickness of SI and different layers are not altered.

(C and D) NADPH-diaphorase (NADPH-d) staining in SI. Dense neuropil staining and barrel pattern are very clear in the wild-type mice (C), whereas in *NR1*$^{-/-}$*LTg*$^{+/+}$ mice, there is a dense band of neuropil staining in layer IV without any segmentation (D).

(E–H) DiI-labeled thalamocortical afferents and their patterned array in SI are best visualized in sections through flattened cortex ([E], wild-type mice). In *NR1*$^{-/-}$*LTg*$^{+/+}$ mice, thalamocortical afferents are confined to SI, but they do not form any pattern (F). Coronal sections through SI also show that thalamic afferents are distributed mainly in layers IV and VI and form patches in layer IV ([G], wild-type mice). In *NR1*$^{-/-}$*LTg*$^{+/+}$ mice, the distribution of thalamic afferents within cortical layers is similar to that of wild-type mice, but they do not segregate in layer IV (H).

Scale bar, 500 μm for (A), (B), (E) and (F); 200 μm for (C), (D), (G), and (H).

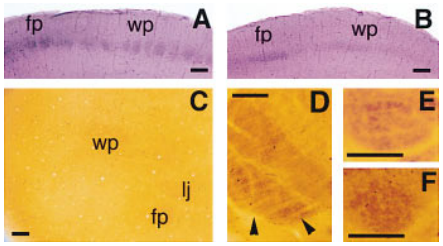

Figure 7. Pattern Formation in an *NR1*$^{-/-}$*LTg*$^{+/-}$ Mouse

(A and B) NADPH-d stained coronal sections through SI. Both of the forepaw (fp) and whisker (wp) regions have clear segmentation in wild-type mice (A), but no such patterning is visible in an *NR1*$^{-/-}$*LTg*$^{+/-}$ mouse (B).

(C and D) CO staining in flattened cortex (C) and coronally sectioned thalamus (D) of *NR1*$^{-/-}$*LTg*$^{+/-}$ mouse show no patterns, including the forepaw area (indicated by arrow heads in [D]) (compare with Figure 5).

(E and F) CO stains of coronally sectioned brainstem. Cu of wild-type mice (E) but not *NR1*$^{-/-}$*LTg*$^{+/-}$ mouse (F) shows forepaw-related segmentation. Scale bars, 200 μm.

not impaired. However, in the mutant mice, whisker-specific patterning as assessed with CO histochemistry and immunohistochemistry for extracellular matrix proteins was absent. This study demonstrated that at the brainstem level, NR1 subunit expression is required for barrelette formation but not for overall topography of trigeminal projections. On the other hand, due to neonatal lethality of *NR1* KO mice, the role of functional NMDA receptors on patterning of somatosensory maps at the level of the thalamus or SI could not be examined. In the present study, we rescued the *NR1* KO mice from neonatal death by introducing *NR1* transgenes. In these mice, development of the somatotopic patterns depended on the level of the expression of the transgenes. In mice with high levels of NR1 expression, apparently normal patterns were formed throughout the somatosensory system. In contrast, the rescued mice with low levels of *NR1* transgene expression lacked somatotopic patterns along the trigeminal pathway from BSTC all the way up to SI. In addition, in a single rescued mouse with a very low level of the transgene expression, the patterns were absent along both the trigeminal and the dorsal column pathways. In all these mice without patterns, axonal projections appeared normal in their density and distribution at all levels of the somatosensory pathway, including SI (Figures 5–7). In a preliminary study, we applied tiny crystals of the lipophilic tracer DiI to nonoverlapping regions of SI and observed discrete, nonoverlapping populations of retrogradely labeled cells in the thalamus (data not shown), suggesting that in these animals as well some level of topography in axonal projections is present. However, detailed electrophysiological and morphological (at the single axon arbor level) studies are required to clearly define the role of NMDA receptors in topographic precision of axonal projections.

The results presented in this paper confirmed and strengthened previous conclusions that a sufficient level of NMDA receptor–mediated activity is required for the formation of barrelettes in BSTC (Li et al., 1994; Kutsuwada et al., 1996). The possibility that the pattern formation in the *NR1* KO mice is delayed rather than blocked entirely is now unlikely, because *NR1*$^{-/-}$*LTg*$^{+/+}$ mice did not exhibit barrelettes even at 4 weeks of age.

It has been previously shown that application of AP5 or TTX (a sodium channel blocker) to the barrel cortex of newborn rats did not affect barrel formation (Chiaia et al., 1992; Schlaggar et al., 1993). This failure may be related to the fact that in normal rats, barrels appear

relatively early after birth, starting at P0 (Schlaggar and O'Leary, 1994). Perhaps, the activity-dependent commitment to form barrels had already taken place before the inhibition of the receptor activity by the applied drugs reached a critical threshold level.

While our results show that NMDA receptor-mediated activity is necessary for pattern formation in the somatosensory brainstem, they do not provide direct evidence for similar mechanisms at the level of the somatosensory thalamus and cortex. Disrupted (ineffective) NMDA receptor function in the brainstem alone can account for the absence of patterns at higher levels. Lesions of the Pr in newborn rats were shown to cause disruption of whisker-related pattern in the thalamus (Killackey and Fleming, 1985). On the other hand, emerging new evidence implicates NMDA receptors in pattern formation in the barrel cortex. For example, a recent study using systemic or local application of NMDA receptor antagonists to neonatal rats found that such pharmacological interventions affect patterning of layer IV granule cells and thalamocortical afferents into barrels as well as down-regulation of the extracellular matrix molecule tenascin from prospective barrel centers (Mitrovic et al., 1996). The lack of barrels in SI of monoamine oxidase A–deficient mice also suggests the operation of an activity-dependent process in barrel formation, because excessive amounts of serotonin in these mice could mediate strong presynaptic inhibitory effects upon thalamocortical transmission (Cases et al., 1996). The present evidence strongly favors NMDA receptor–mediated cellular mechanisms in formation of somatotopic patterns in the neocortex as well.

How does the NMDA receptor–mediated activity serve pattern formation in the somatosensory system? It is likely that NMDA receptor-dependent associative processes such as long-term potentiation (LTP) and/or long-term depression (LTD) are involved in the consolidation of synapses that receive coordinated inputs and elimination of synapses that receive uncoordinated inputs during development. At thalamocortical synapses of the rat SI, NMDA receptor–dependent LTP has been reported to be inducible during the first postnatal week (Crair and Malenka, 1995; Isaac et al., 1997). In addition, a preliminary study indicates that the developmental periods during which LTD and LTP are inducible correspond to those in which barrelettes are formed and consolidated, respectively (Erzurumlu et al., 1997, Soc. Neurosci., abstract).

The NR1 subunit is expressed widely in the developing and adult brains (Watanabe et al., 1992; Monyer et al., 1994), but there exist at least seven splice variants, each of which has distinct pharmacological and physiological properties (Traynelis et al., 1995; Zukin and Bennett, 1995; Ehlers et al., 1996). The expression of NR1 splice variants is differentially regulated in various brain regions during development (Hofer et al., 1994; Laurie and Seeburg, 1994; Laurie et al., 1995; Zhong et al., 1995). In addition, one NMDA receptor complex may contain two different NR1 splice variants (Blahos and Wenthold, 1996). Thus, the contribution of NR1 to the functional diversity of NMDA receptors throughout the developing and adult brain can potentially be substantial. It is therefore interesting that a single splice variant, NR1-1a, is capable of rescuing the *NR1*$^{-/-}$ mice and restoring apparently normal somatotopic patterns when it is expressed at sufficiently high levels.

Experimental Procedures

Transgenic Constructs

The *NR1-1a* cDNA (*pJS1* clone: Sullivan et al., 1994) was verified by restriction mapping and sequence analysis of critical regions (e.g., the initiation codon, the stop codon, N/Q/R site, alternative exons) and used for making the transgenes *pCAG-NR1* and *pNR2D-NR1*. *pCAG-NR1*: *pMSG-NR1* was prepared by inserting the BamHI-NotI fragment (*NR1-1a* cDNA) of *pJS1* clone into the XhoI site of the *pMSG* vector (Pharmacia) by blunt end ligation. The *pCAG-NR1* construct was prepared by inserting the SalI-BamHI fragment of *pMSG-NR1* into the XhoI-BamHI site of the *pCAGGS* vector (Niwa et al., 1991). *pCAG-NR1* was digested with SalI and BamHI and purified away from plasmid sequence by gel electrophoresis to prepare a linear construct for injection. *pNR2D-NR1*: genomic Southern hybridization revealed the presence of EcoRI sites at 23 kb upstream and 8 kb downstream of the initiation codon of the *NR2D* gene (T. I. and S. T., unpublished data). A cosmid library was made by inserting EcoRI-digested genomic DNA of D3 ES cells into the EcoRI site of the *CosPE* vector. The *CosPE* vector was made from *SuperCos* vector (Stratagene) and had an EcoRI site and a PacI site instead of a multicloning site (T. I. and S. T., unpublished data). The *pCosPE-NR2D* clone, which has a 31 kb EcoRI fragment containing the *NR2D* initiation codon, was isolated from the cosmid library. The *pCosPE-NR2D* clone had a PacI site upstream of the insert. About 150 bp sequences containing the *NR2D* initiation codon (between ApaI and NotI sites) were deleted from *pCosPE-NR2D*, and the SalI-BamHI fragment of *pMSG-NR1* was inserted in right direction through several steps of ligation to generate the *pNR2D-NR1* construct. A 31 kb linearized DNA was purified away from the vector sequence by digesting *pNR2D-NR1* with PacI and MluI.

Generation of Transgenic Mice

The transgenic founder mice were generated by microinjection of linearized constructs into C57Bl/6 × CBA F2 (BCF2) or C57Bl/6 × BCF1 fertilized eggs as described (Hogan et al., 1986). *NR1*$^{+/-}$ mice (Li et al., 1994), which were backcrossed 7–8 times to C57Bl/6 (B6) strain (gifts of Dr. Y. Li), were used for the initial mating with founder mice. Thereafter, offspring were maintained on mixed genetic background between B6 and CBA. Genotyping of the mice was initially done by Southern blotting of tail DNA. Tail DNA was digested with EcoRI and hybridized with probe-R (AvrII-SphI 0.4 kb from *pMSG-NR1*), which is specific to the deleted region of the mutant *NR1* allele, and probe-N (1.8 kb EcoRI-HindIII fragment), corresponding to the phosphoglycerate kinase (*PGK*) promoter/*neo* gene. Probe-R detects 17 kb band for wild-type *NR1* allele (Li et al., 1994) and 1.9 kb for the *CAG-NR1* and the *NR2D-NR1* transgenes (Figure 1A). Probe-N detects 12 kb band for the mutant *NR1* allele (Li et al., 1994). Later mice were typed by PCR analysis with a set of *neo1* primers (Li et al., 1994) and a set of *NR1* primers (5′-AGCCCTTCAAG TACCAGGGCCTGAC and 5′-AGCGGTCCAGCAGGTACAGCAT CAC, 160 bp, 240 bp, and no PCR products for transgenic, wild-type, and mutant *NR1*, respectively). Homozygosity of transgenic mice was determined by Southern blotting. In some cases, results were confirmed by test mating with nontransgenic mice. All animal handling was in accordance with a protocol approved by the Massachusetts Institute of Technology Animal Use and Care Committee.

Northern Blot Analysis

Mice were sacrificed by cervical dislocation, and various brain regions were quickly dissected and frozen immediately in liquid nitrogen. Total RNA was purified using Tri-reagent (Molecular Research Center). Twenty micrograms of total RNA were loaded per lane, separated on 1% agarose formaldehyde gels, blotted to a Hybond-N nylon membrane (Amersham), and hybridized with transgene-specific probe (probe-T) (0.9 kb XhoI-BamHI fragment of *pMSG*) and G3PDH probe (Clontech). Quantification was done with a Fujix Bio-Imaging Analyzer.

In Situ Hybridization

In situ hybridization was done according to the protocol described by Simmons et al. (1989) with modification. Frozen brains (P8) and heads (P0) were cut at a thickness of 14 μm in the sagittal or coronal planes in a cryostat. Sections were postfixed in 4% paraformaldehyde in phosphate-buffered saline (pH 7.2) for 20 min before pretreatment. Hybridization was done at 52°C for 20 hr in hybridization buffer with 5×10^5 cpm of ^{35}S-labeled RNA probe. Sections were washed in a series of SSC/DTT buffers of increasing stringency after RNase A treatment. The final wash was done in 0.1× SSC, 1 mM DTT at 60°C for 30 min. The sections were exposed to hyper-beta max (Amersham) for 5 days and were then dipped in Kodak NTB2 nuclear emulsion followed by exposure for 4 weeks. After development, sections were stained with 0.25% thionin. Antisense probe was made from *pSP72-ASp* clone using SP6 RNA polymerase. *pSP72-ASp* was generated by inserting AvrII-SphI 0.4 kb (probe-R) of *NR1* cDNA into XbaI-SphI sites of pSP72 (Promega). Probe-R can detect all splice variants of the *NR1* gene. Expression patterns and levels were ascertained by several sets of reactions using one to three each of wild-type, *NR1*$^{-/-}$*HTg*$^{+/-}$, and *NR1*$^{-/-}$*LTg*$^{+/+}$ brains at P0 and P8. Brains of P0 *NR1* KO mice were used as negative control.

For quantitation, we used sections that were processed simultaneously and exposed to an X-ray film. The signal levels in a given region were obtained as the mean optical density and standard deviation (SD) calculated from two to three measurements from different sections of each brain (using the N.I.H. Image 1.6).

Electrophysiology

Mice (9–12 days old) were anesthetized with ice and sacrificed by decapitation. The brain was quickly removed and submerged in artificial cerebrospinal fluid (ACSF) solution at ~4°C for ~3 min. The ACSF contained (in mM): 124 NaCl, 26 NaH_2CO_3, 10 D-glucose, 5 KCl, 2 $CaCl_2$, 2 $MgSO_4$, 1.2 NaH_2PO_4 (pH 7.2), and was oxygenated with a 95% O_2-5% CO_2 gas mixture. Thalamocortical slices (350 μm thick) were prepared according to the protocol of Agmon and Connors (1991) using a Vibratome. Slices were transferred to a holding chamber and kept at 37°C for the first ~45 min and at room temperature for the rest of the experiment. Recordings were made 2–6 hr after dissection. A single slice was transferred to a submerged recording chamber and was bathed with rapidly flowing (1 ml/min) oxygenated ACSF containing picrotoxin (100 μM). Bath temperature was maintained at 30°C–32°C with a heating controller unit (TC-324, Warner). The recording chamber was mounted on an upright fixed-stage microscope (Zeiss).

Intracellular patch-clamp recordings, in the whole-cell mode, were conducted (reviewed by Sakmann and Stuart, 1995). Infrared illumination coupled to DIC optics with a 40× water immersion objective (Zeiss) enabled us to visualize the cell bodies of layer IV neurons in the superficial layer of the slice, allowing assessment of the health of the slice and recordings of identified neurons under visual guidance (Edwards et al., 1989; Sakmann and Stuart, 1995). Patch electrodes (resistance, 5–7 MΩ) were pulled from thin-walled glass pipettes (150F-4, WPI) and filled with internal solution, containing (in mM): 140 K-gluconate, 1.1 EGTA, 0.1 $CaCl_2$, 10 HEPES, 2 Mg-ATP, 1 $MgCl_2$, and 0.3 Na-GTP (pH 7.2). Access resistances were measured regularly during recording (typical values were 10–20 MΩ). Synaptic responses were evoked by stimulating with a bipolar Pt/Ir electrode placed in the thalamus (Figure 4A). Stimuli (50 μs, 0.1–0.7 mA) produced EPSCs, which were amplified with an Axopatch 1D amplifier (Axon Instruments), digitized with an A/D board (Digidata 1200A, Axon), and analyzed on-line by *adslice* data collection software (written by P. T. H). The NMDA currents were isolated pharmacologically by adding the following to the ACSF: the AMPA receptor antagonist CNQX (20 μM) or DNQX (10 μM), picrotoxin (100 μM), 2-OH-saclofen (200 μM), glycine (1 μM), and by removing Mg^{2+} from the ACSF. The AMPA currents were isolated by adding the same solution, except that the AMPA antagonist was replaced by AP5 (50 μM).

Histology

Cytochrome oxidase histochemistry was performed on 4% paraformaldehyde-fixed, frozen sectioned 90 μm thick brain sections. Sections were incubated in 4 g of sucrose, 50 mg of cytochrome C, and 50 mg of diaminobenzidine in 100 ml of phosphate buffer at 37°C in a shaker incubator for 3–4 hr. Sections were then rinsed in phosphate buffer, mounted on subbed slides, and coverslipped with an aqueous medium containing gelatin and glycerol. Brains from different groups of mice were cut and reacted the same day using the same solutions in a blind fashion.

For NADPH-diaphorase staining, brain sections prepared the same way as for CO histochemistry were incubated in a solution of 5 mg of nitroblue tetrazolium, 20 mg of NADPH (β-nicotinamide adenine dinucleotide phosphate) in 20 ml of Tris buffer (pH 7.1) at 37°C in a shaker incubator for 2–3 hr. Sections were then rinsed in Tris buffer, mounted onto slides, and coverslipped with an aqueous medium.

To visualize axonal projection patterns along the somatosensory pathway, crystals of the lipophilic tracer DiI (Molecular Probes) were inserted into the trigeminal ganglion, principal nucleus, or VPM in paraformaldehyde-fixed brains. Labeled brains were kept at 37°C for 2–4 weeks and then sectioned in a Vibratome, and labeling patterns were photographically documented using epifluorescence and a rhodamine filter.

To examine cortical cytoarchitecture, one wild-type and one *NR1*$^{-/-}$*LTg*$^{+/+}$ brain (P8) were embedded in paraffin, sectioned at 15 μm in the coronal plane on a rotary microtome, and stained with cresyl violet.

Acknowledgments

We thank Dr. Yuqing Li for providing *NR1* heterozygous mutant mice and help; Dr. Mazahir Hasan for suggestions and critical discussion throughout this project; Heather Hinds for comments on the manuscript; Dr. Jun-ichi Miyazaki for providing *pCAGGS* clone; Drs. Jane M. Sullivan and Stephen F. Heinemann for providing *pJS1* clone; and Turker Ulupinar for help with preparation of figures. We also thank the members of Tonegawa laboratory for their contribution. T. I. was supported by fellowships from the Human Frontier Science Program and the Uehara Memorial Foundation. P. T. H. was supported by the Pew Latin American Fellows Program. T. S. was supported by the Stanley Foundation. E. U. was supported by the Higher Education Council of Turkey and Osmangazi Univ. This work was supported by NIH grant NS32925, by gifts from the Shionogi Institute for Medical Science and Amgen, Inc. (all to S. T.), and by NIH grant NS32195 (to R. S. E.).

Received July 22, 1997; revised November 19, 1997.

References

Agmon, A., and Connors, B.W. (1991). Thalamocortical responses of mouse somatosensory (barrel) cortex in vitro. Neuroscience *41*, 365–379.

Belford, G.R., and Killackey, H.P. (1978). Anatomical correlates of the forelimb in the ventrobasal complex and the cuneate nucleus of the neonatal rat. Brain Res. *158*, 450–455.

Belford, G.R., and Killackey, H.P. (1979). Vibrissae representation in subcortical trigeminal centers of the neonatal rat. J. Comp. Neurol. *183*, 305–322.

Blahos, J., II, and Wenthold, R.J. (1996). Relationship between N-methyl-D-aspartate receptor NR1 splice variants and NR2 subunits. J. Biol. Chem. *271*, 15669–15674.

Cases, O., Vitalis, T., Seif, I., De Maeyer, E., Sotelo, C., and Gaspar, P. (1996). Lack of barrels in the somatosensory cortex of monoamine oxidase A-deficient mice: role of a serotonin excess during the critical period. Neuron *16*, 297–307.

Chiaia, N.L., Fish, S.E., Bauer, W.R., Bennett-Clarke, C.A., and Rhodes, R.W. (1992). Postnatal blockade of cortical activity by tetrodotoxin does not disrupt the formation of vibrissae-related patterns in the rat's somatosensory cortex. Dev. Brain Res. *66*, 244–250.

Crair, M.C., and Malenka, R.C. (1995). A critical period for long-term potentiation at thalamocortical synapses. Nature *375*, 325–328.

Cramer, K.S., and Sur, M. (1995). Activity-dependent remodeling of

connections in the mammalian visual system. Curr. Opin. Neurobiol. *5*, 106–111.

Dawson, D.R., and Killackey, H.P. (1987). The organization and mutability of the forepaw and hindpaw representations in the somatosensory cortex of the neonatal rat. J. Comp. Neurol. *256*, 246–256.

Edwards, F., Konnerth, A., Sakmann, B., and Takahashi, T. (1989). A thin slice preparation for patch clamp recordings from neurones of the mammalian central nervous system. Pflügers Arch. *414*, 600–612.

Ehlers, M.D., Zhang, S., Bernhardt, J.P., and Huganir, R.L. (1996). Inactivation of NMDA receptors by direct interaction of calmodulin with the NR1 subunit. Cell *84*, 745–755.

Forrest, D., Yuzaki, M., Soares, H.D., Ng, L., Luk, D.C., Sheng, M., Stewart, C.L., Morgan, J.I., Connor, J.A., and Curran, T. (1994). Targeted disruption of NMDA receptor 1 gene abolishes NMDA response and results in neonatal death. Neuron *13*, 325–338.

Fox, K., Schlaggar, B.L., Glazewski, S., and O'Leary, D.D.M. (1996). Glutamate receptor blockade at cortical synapses disrupts development of thalamocortical and columnar organization in somatosensory cortex. Proc. Natl. Acad. Sci. USA *93*, 5584–5589.

Goodman, C.S., and Shatz, C.J. (1993). Developmental mechanisms that generate precise patterns of neural connectivity. Cell *72*/Neuron *10* (Suppl.), 77–98.

Hahm, J.-O., Langdon, R.B., and Sur, M. (1991). Disruption of retinogeniculate afferent segregation by antagonists to NMDA receptors. Nature *351*, 568–570.

Henderson, T.A., Woolsey, T.A., and Jacquin, M.F. (1992). Infraorbital nerve blockade from the birth does not disrupt central trigeminal pattern formation in the rat. Dev. Brain Res. *66*, 146–152.

Hofer, M., Prusky, G.T., and Constantine-Paton, M. (1994). Regulation of NMDA receptor mRNA during visual map formation and after receptor blockade. J. Neurochem. *62*, 2300–2307.

Hogan, B., Constantin, F., and Lacy, E. (1986). Manipulating the Mouse Embryo: A Laboratory Manual (Plainview, NY: Cold Spring Harbor Press).

Isaac, J.T.R., Crair, M.C., Nicoll, R.A., and Malenka, R.C. (1997). Silent synapses during development of thalamocortical inputs. Neuron *18*, 269–280.

Katz, L.C., and Shatz, C.J. (1996). Synaptic activity and the construction of cortical circuits. Science *274*, 1133–1138.

Killackey, H.P., and Fleming, K. (1985). The role of the principal sensory nucleus in central trigeminal pattern formation. Dev. Brain Res. *22*, 141–145.

Killackey, H.P., Jacquin, M.F., and Rhodes, R.W. (1990). Development of somatosensory system structures. In Development of Sensory System in Mammals, E.J. Coleman, ed. (New York: Wiley), pp. 403–429.

Kutsuwada, T., Sakimura, K., Manabe, T., Takayama, C., Katakura, N., Kushiya, E., Natsume, R., Watanabe, M., Inoue, Y., Yagi, T., et al. (1996). Impairment of sucking response, trigeminal neuronal pattern formation, and hippocampal LTD in NMDA receptor ϵ2 subunit mutant mice. Neuron *16*, 333–344.

Laurie, D.J., and Seeburg, P.H. (1994). Regional and developmental heterogeneity in splicing of the rat brain NMDAR1 mRNA. J. Neurosci. *14*, 3180–3194.

Laurie, D.J., Putzke, J., Zieglansberger, W., Seeburg, P.H., and Tolle, T.R. (1995). The distribution of splice variants of the NMDAR1 subunit mRNA in adult rat brain. Mol. Brain Res. *32*, 94–108.

Li, Y., Erzurumlu, R.S., Chen, C., Jhaveri, S., and Tonegawa, S. (1994). Whisker-related neuronal patterns fail to develop in the trigeminal brainstem nuclei of NMDAR1 knockout mice. Cell *76*, 427–437.

Ma, P.K., and Woolsey, T.A. (1984). Cytoarchitectonic correlates of the vibrissae in the medullary trigeminal complex of the mouse. Brain Res. *306*, 374–379.

Mitrovic, N., Mohajeri, H., and Schachner, M. (1996). Effects of NMDA receptor blockade in the developing rat somatosensory cortex on the expression of the glia-derived extracellular matrix glycoprotein Tenascin-C. Eur. J. Neurosci. *8*, 1793–1802.

Monyer, H., Burnashev, N., Laurie, D.J., Sakmann, B., and Seeburg, P.H. (1994). Development and regional expression in the rat brain and functional properties of four NMDA receptors. Neuron *12*, 529–540.

Nakanishi, S. (1992). Molecular diversity of glutamate receptors and implications for brain function. Science *258*, 597–603.

Niwa, H., Yamamura, K., and Miyazaki, J. (1991). Efficient selection for high-expression transfectants by a novel eukaryotic vector. Gene *108*, 193–200.

O'Leary, D.D.M., Ruff, N.L., and Dyck, R.H. (1994). Development, critical period plasticity, and adult reorganizations of mammalian somatosensory system. Curr. Opin. Neurobiol. *4*, 535–544.

Sakmann, B., and Stuart, G. (1995). Patch-pipette recordings from the soma, dendrites, and axons of neurons in brain slices. In Single-Channel Recording, 2nd Ed., B. Sakmann and E. Neher, eds. (New York: Plenum Press), pp. 199–211.

Schlaggar, B.L., and O'Leary, D.D.M. (1994). Early development of the somatotopic map and barrel patterning in rat somatosensory cortex. J. Comp. Neurol. *346*, 80–96.

Schlaggar, B.L., Fox, K., and O'Leary, D.D.M. (1993). Postsynaptic control of plasticity in developing somatosensory cortex. Nature *364*, 623–626.

Shatz, C.J., and Stryker, M.P. (1988). Prenatal tetrodotoxin infusion blocks segregation of retinogeniculate afferents. Science *242*, 87–89.

Simmons, D.M., Arriza, J.L., and Swanson, L.W. (1989). A complete protocol for in situ hybridization of messenger RNAs in brain and other tissues with radiolabeled single-stranded RNA probes. J. Histotech. *12*, 169–181.

Stryker, M.P., and Harris, W.A. (1986). Binocular impulse blockade prevents the formation of ocular dominance columns in cat visual cortex. J. Neurosci. *6*, 2117–2133.

Sullivan, J.M., Traynelis, S.F., Chen, H.-S.V., Escober, W., Heinemann, S., and Lipton, S.A. (1994). Identification of two cysteine residues that are required for redox modulation of the NMDA subtype of glutamate receptor. Neuron *13*, 929–936.

Traynelis, S.T., Hartley, M., and Heinemann, S.F. (1995). Control of proton sensitivity of the NMDA receptor by RNA splicing and polyamines. Science *268*, 873–876.

Van der Loos, H. (1976). Barreloids in mouse somatosensory thalamus. Neurosci. Lett. *2*, 1–6.

Watanabe, M., Inoue, Y., Sakimura, K., and Mishina, M. (1992). Developmental changes in distribution of NMDA receptor channel subunit mRNAs. NeuroReport *3*, 1138–1140.

Woolsey, T.A., and Van der Loos, H. (1970). The structural organization of layer IV in the somatosensory region (SI) of the mouse cerebral cortex. Brain Res. *17*, 205–242.

Zhong, J., Carrozza, D.P., Williams, K., Pritchett, D.B., and Molinoff, P.B. (1995). Expression of mRNAs encoding subunits of the NMDA receptor in developing rat brain. J. Neurochem. *64*, 531–539.

Zukin, R.S., and Bennett, M.V.L. (1995). Alternative splice isoforms of the NMDAR1 receptor subunit. Trends Neurosci. *18*, 306–313.